NUMERICAL SIMULATIONS OF SPONTANEOUS IGNITION OF HIGH-PRESSURE HYDROGEN BASED ON DETAILED CHEMICAL KINETICS

Terashima, H.[1], Koshi M.[1], Miwada, C.[2], Mogi, T.[2], and Dobashi, R.[2]
[1] **Institute of Engineering Innovation, University of Tokyo, 2-11-16 Yayoi, Bunkyo, Tokyo, 113-8656, Japan, htera@rocketlab.t.u-tokyo.ac.jp**
[2] **Dept. of Chemical System Engineering, University of Tokyo, 7-3-1 Hongo, Bunkyo, Tokyo, 113-8656, Japan**

ABSTRACT

A two-dimensional (2-D) simulation of spontaneous ignition of high-pressure hydrogen in a length of duct is conducted in order to explore its underlying ignition mechanisms. The present study adopts a 2-D rectangular duct (i.e., not axisymmetric geometry) and focuses on the effects of initial diaphragm shape on the spontaneous ignitions. The Navier-Stokes equations with a detailed chemical kinetics mechanism are solved in a manner of direct numerical simulation. The detailed mechanisms of spontaneous ignition are discussed for each initial diaphragm shape. For a straight diaphragm shape, it is found that the ignition occurs only near the wall due to the adiabatic wall condition, while the three ignition events: ignitions due to leading shock wave reflection at the wall, hydrogen penetration into shock-heated air near the wall, and deep penetration of hydrogen into shock-heated air behind the leading shock wave are identified for a largely deformed diaphragm shape.

1.0 INTRODUCTION

When highly pressurized hydrogen is released into air, spontaneous ignition may occur due to the production of shock-heated gas and sufficient mixing between hydrogen and air, potentially leading to significant hazardous incidences. Recently, use of high-pressure hydrogen as high as 700 atm has been considered as a storage pressure in hydrogen gas stations for the operation of fuel-cell vehicles. Thus, in order to establish reliable risk assessment or safety guideline on the operation of high-pressure hydrogen, issues related to the spontaneous ignition have to be fundamentally clarified.

Following a pioneering experimental work by Wolanski and Wojcicki [1], several experimental works [2-5] have been performed for spontaneous ignition of high-pressure hydrogen released into air. Generally, the experimental data have confirmed that increasing the pressure of hydrogen decreases the distance from the burst location to the hydrogen ignition. Dryer et al. [2] demonstrated the occurrence of spontaneous ignition by high-pressure hydrogen releases from a tube, and provided a potential scenario of the mixing phenomena to result in the spontaneous ignition. Golub et al. [3] identified the importance of the cross section shape of the tube on the hydrogen self-ignition. They also numerically simulated the influence of the boundary layer on governing ignition mechanisms. Mogi et al. [4] experimentally observed that the possibility of self-ignition increased with increasing length of the discharge tube. A latest effort by Kim et al. [5] provided flow visualization inside a tube using Shadowgraph in addition to the measurement with pressure and light sensors.

While experimental works have been successfully dedicated to understand the spontaneous ignition mechanisms, for the last five years, with help of growing computer powers, numerical simulations have been conducted to further identify detailed mechanisms of spontaneous ignition of high-pressure hydrogen inside the tubes. Wen et al. [6] performed a parametric study on spontaneous ignition of pressurized hydrogen release through a length of tube in a manner of two-dimensional direct numerical simulation (DNS). The effects of rupture time, release pressure, and tube length and diameter on the spontaneous ignition were comprehensively investigated. For example, it was suggested that slower rupturing process and smaller ratio of the tube length and diameter help to avoid the likelihood of spontaneous ignition. Wen et al. [7], following their previous study [6], also found the important role of the finite rupture process on numerically predicting the spontaneous ignition. The

finite rupture process provides accurate predictions of shock velocity and turbulent mixing at contact region, influencing the ignition mechanism.

Lee and Jeung [8] conducted a two-dimensional DNS with detailed chemical kinetics, using a realistic rupture process of the pressure boundary. They simulated the detailed mechanism of the early ignition near the boundary layer and the following spontaneous ignition due to the sufficient mixing of the expanding hydrogen jet and shock-heated air in the downstream region. Yamada et al. [9], using DNS, indicated a possibility of an auto-ignition induced by vortices behind the shock wave in a long tube, suggesting that the understanding of the phenomenon with vortices near the contact region is necessary.

In contrast with use of DNS, a large-eddy simulation (LES) model [10] was applied to the spontaneous ignition phenomena with a relatively coarse grid resolution to the DNS studies. The results were in agreement with experimental data on the distance for spontaneous ignition from the rupture disk, demonstrating the validity of their LES model for the prediction of spontaneous ignition, while the detailed unsteady flow structures were seemingly lost.

Following several successful numerical studies of spontaneous ignition of pressurized hydrogen released into the tubes, in this study, we also perform a numerical simulation of spontaneous ignition of highly pressurized hydrogen inside a two-dimensional duct in a manner of DNS. Especially, the present study carries out a detailed investigation, focusing on the effect of initial diaphragm shape on spontaneous ignition mechanisms, while earlier relevant studies [6,8] investigated the effect of rupture rate, using only one initial diaphragm shape with curvature. Further, a full two-dimensional domain, i.e., no axisymmetric geometry is adopted in order to explore possible mechanisms of spontaneous ignition in a different geometry, while most of earlier studies have used an axisymmetric assumption.

2.0 NUMEICAL METHOD

The Navier-Stokes equations with the conservation equations of each chemical species are used as the governing equations, where the thermally perfect gas equation of state is applied. The governing equations in this study are thus written as:

$$\partial \rho / \partial t + \nabla \cdot \rho \boldsymbol{u} = 0, \tag{1}$$

$$\partial \rho \boldsymbol{u} / \partial t + \nabla \cdot (\rho \boldsymbol{u} \otimes \boldsymbol{u} + p \boldsymbol{\delta} - \boldsymbol{\tau}) = 0, \tag{2}$$

$$\partial E / \partial t + \nabla \cdot \big((E + p)\boldsymbol{u} - \boldsymbol{\tau} \cdot \boldsymbol{u} - \boldsymbol{q} \big) = 0, \tag{3}$$

$$\partial \rho Y_s / \partial t + \nabla \cdot (\rho Y_s \boldsymbol{u}) - \nabla (\rho D_s \nabla Y_s) = \dot{\omega}_s, \tag{4}$$

where ρ - density; $\boldsymbol{u}$ - velocity vector; p - pressure; E - total energy; $\boldsymbol{\tau}$ - viscous stress tensor; $\boldsymbol{q}$ - heat flux vector; $\boldsymbol{\delta}$ - unit tensor; Y_s - mass fraction of species s; D_s - diffusion coefficient of species s; $\dot{\omega}_s$ - reaction rate of species s. Here $s = 1 \sim N$ where N is the total number of species.

The above equations (1) ~ (4) are solved in the operator-splitting form in order to efficiently handle a wide range of timescales in problems, i.e., the fluid and chemical reaction parts are solved separately in terms of the time integrations. The fluid part in Eq. (1) ~ (4) is solved under an assumption that the chemical reactions are frozen, i.e., $\dot{\omega}_s = 0$, while the chemical reaction is treated under an assumption that the volume and internal energy of fluids are constant, and the spatial derivatives in Eq. (1) ~ (4) are neglected. The governing equations for the chemical reactions are thus derived as:

$$\mathrm{d} Y_s / \mathrm{d} t = \dot{\omega}_s / \rho, \tag{5}$$

$$\mathrm{d} T / \mathrm{d} t = - \sum_{s=1}^{N} e_s \, \dot{\omega}_s / (\rho c_v), \tag{6}$$

where T - temperature; e_s - internal energy of species; c_v - specific heats at constant volume.

The primitive variables such as temperature, mass fractions, pressure, density are exchanged between the fluid equations (1) ~ (4) ($\dot{\omega}_s = 0$) and the chemical reaction equations (5) ~ (6) at each time step.

For the Navier-Stokes equations without the chemical source terms ($\dot{\omega}_s = 0$), the numerical flux is evaluated by the Harten-Lax-van Leer-Contact (HLLC) scheme [11] with a modification of [12]. Higher-order spatial accuracy is achieved using the Monotone Upstream-centred Schemes for Conservation Law (MUSCL) with a primitive variable interpolation and the minmod limiter [13]. The viscous, heat conductivity, and diffusion terms are evaluated by the second-order central differencing. The time integration is done with the third-order Total Variation Diminishing (TVD) Runge-Kutta scheme [14]. These numerical techniques have been used successfully for a wide range of compressible flow simulations. In this study, no sub-grid scale model is used.

The single component viscosities and binary diffusion coefficients are calculated by the standard kinetic theory expression of Hirschfelder [15], and the model of Warnatz [16] is used for the single component thermal conductivity. The mixture-averaged viscosity is given by a formula of Bird [17] and the mixture-averaged thermal conductivity is evaluated from a formula of Mathur et al. [18]. The mixture-averaged model by Bird et al. [17] is used for the mixture diffusion coefficient. The Soret effect for species transport and the Dufour effect for heat transport are both neglected in this study.

For efficiently conducting the time integration of the reaction equations (5)~(6), while avoiding the stiffness, a dynamic multi-time scale (MTS) method [19] is applied in this study. MTS, which is in a class with explicit integration methods, alleviates the stiffness of chemical reaction equations by categorizing chemical species based on the characteristic times. Note that, for multidimensional reacting flow problems (where the chemical reaction equations are solved at each grid point), implicit Ordinary Differential Equation (ODE) integration methods, e.g., Variable coefficient ODE (VODE) [20] may be inefficient because of the start-up costs and matrix operations.

A detailed chemical reaction mechanism of hydrogen (called UT-JAXA) proposed by one of the authors [21] is used to compute the chemical reaction rates. The present mechanism consists of 9 species (H_2, H, O_2, O, OH, HO_2, H_2O_2, H_2O, and N_2) and 34 elementary reactions. The accuracy of the reaction model is validated for a wide range of pressure conditions.

3.0 RESULTS AND DISCUSSIONS

3.1 Computational Conditions

A schematic of the problem is shown in Fig. 1. A two-dimensional rectangular duct of 10 cm × 0.5 cm is considered, where high-pressure hydrogen of 100.0 atm is filled in the left region and atmospheric air (O_2/N_2=1.00/3.76 for the mole fraction) of 1.0 atm is filled in the right region. An initial temperature is 300 K for the whole region. Adiabatic wall condition is assumed on the upper and lower boundaries (note that no axisymmetric condition is used). On the left and right boundaries, the conservative variables are simply extrapolated. The computational grid is constructed with a uniform grid size of 12.5 μm based on several earlier studies [6-9], except for the left region of 0.0 to 4.0 cm where non-uniform grid sizes are used for saving computing resources. A grid convergence study is performed in order to confirm the validity of the present simulation, which is described below.

The present study investigates the effect of initial diaphragm shape (in other words, initial pressure boundary) on mechanism of spontaneous ignition of hydrogen-air mixture inside the duct. The initial diaphragm shape is generated as:

$$x = x_c + \delta \Delta h \cos(2\pi y / \Delta h), \tag{7}$$

where $x_c = 5$ is the position of the initial diaphragm in the x-coordinate, $\Delta h = 0.5$ is the height of the computational domain, and δ is the amplitude of initial diaphragm shape. The effect of initial diaphragm shape is investigated by using the three values of δ: 0.0, 0.05, and 0.1 (convex in the x

direction) in Eq. (7): larger δ, larger curvature of initial diaphragm. We assume that the initial diaphragm is instantly ruptured; the rupture process of the initial boundary is not considered, although the importance on the spontaneous ignition was reported in earlier studies [6,7].
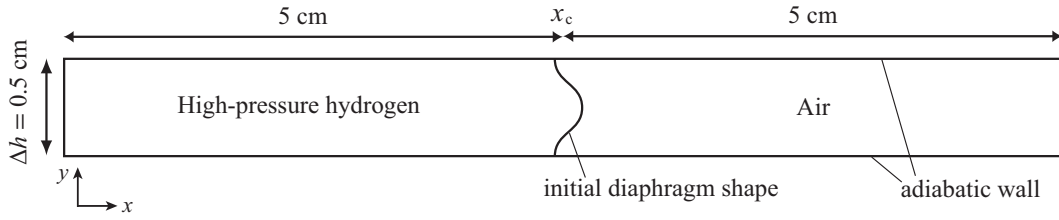

Figure 1. Schematic of computational domain and initial diaphragm shape (not to scale)

3.2 Preliminary 0-D and 1-D studies and validation

At first, 0- and 1-dimensional simulations are conducted to preliminary get some insights into the spontaneous ignition of high-pressure hydrogen in an idealized situation. Figure 2 shows the pressure and temperature profiles at $t = 30.0\ \mu s$ in the one-dimensional shock tube problem using three grid resolutions. The conditions are the same as that described in Fig. 1 with no upper and lower adiabatic walls. It is shown that no ignition occurs until $t = 30.0\ \mu s$ with any grids used.
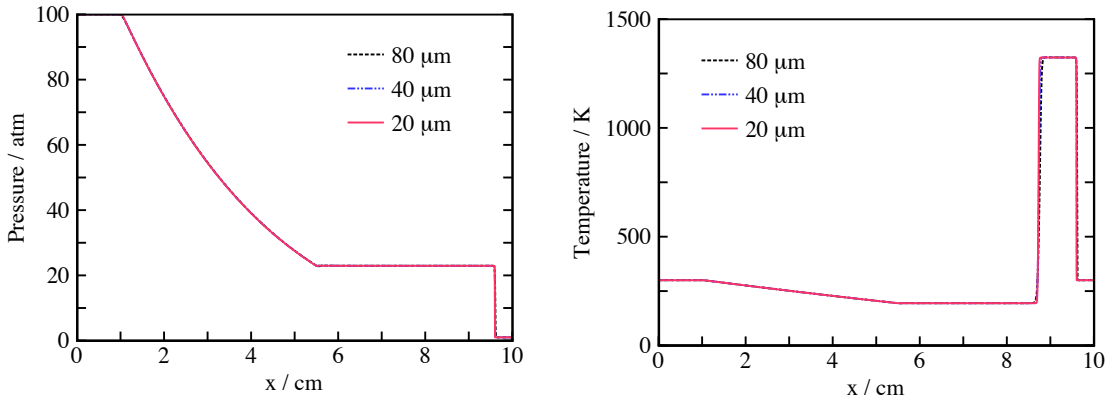
Figure 2. Pressure and temperature profiles at $t = 30.0\ \mu s$ in one-dimensional problem

From the one-dimensional simulation, the pressure and temperature behind the shock wave are found to be about 23 atm and 1320 K, respectively. Based on those values, a 0-dimensional ignition problem, i.e., Eq. (5) ~ (6), is solved to assess possible ignition delay times using the equivalence ratio of 1.0, i.e., hydrogen and air are assumed to be perfectly mixed. Figure 3 shows the time histories of temperature with an initial pressure of 20 atm and three initial temperatures of 1250, 1275, and 1300 K. The results show that the ignition occurs at less than 5 μs in the case of 1300 K, and even with the lowest initial temperature of 1250 K the ignition occurs at only about 20 μs, which indicates that an ignition could potentially occur in the present one-dimensional problem, if hydrogen and air were sufficiently mixed. Thus, if spontaneous ignition occurred under the condition and geometry used here, mixing mechanism between hydrogen and air has to be enhanced by, for example, vortices or boundary layers.

To demonstrate the validity of present numerical method, a one-dimensional shock tube problem is solved with a different condition. High-pressure hydrogen of 86.1 atm is filled in the left region and the length of duct is extended to 40 cm, while the other conditions are kept to be same. The present method using a grid size of 20 μm predicts that the temperature starts to increase by the chemical reaction at the distance of about 23.5 cm from the initial diaphragm position, and the subsequent

ignition (the temperature goes over 2000 K) occurs at the distance of 25.8 cm, which is a comparable result with the critical distances of 24.3 cm reported in the earlier study [8].
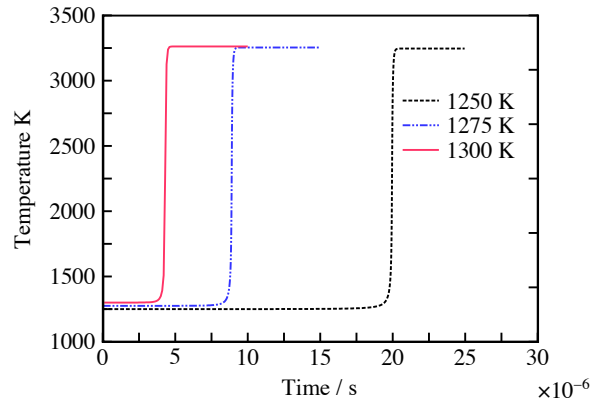

Figure 3. Comparison of ignition delay times with three different initial temperature conditions in 0-dimensional ignition problem

3.3 Grid convergence study on 2-D simulation

A grid convergence study is performed to check the grid resolution for properly resolving the two-dimensional flow fields. Three grids with the minimum grid sizes of $\Delta s = 25$ μm, 17 μm, and 12.5 μm (which are proportional to the square of 2) are used for this investigation, while earlier studies have adopted the grid sizes in the range from 15 to 45 μm. The initial diaphragm shape is generated with δ = 0.1 in Eq. (7).

Figure 4 shows the time history of an area, which is defined as the summation of the area above 2000 K normalized by the half area of the whole region: 5×0.5 cm^2 (hereafter, this defined area is denoted as the 2000 K area rate) One can see that the profile with the grid size of 17 μm is similar to that with 12.5 μm, while the coarsest grid resolution of 25 μm overestimates the area above 2000 K, i.e., the ignition occurs at larger area compared to the other two grids. This may suggest that insufficient grid resolution tends to induce spurious ignitions, probably due to excessive artificial diffusions at mixing regions. Figure 5 presents the temperature and the H$_2$ mass fraction distributions at $t = 20.1$ μs with the three different grids. While the overall structures of the temperature and H$_2$ distributions are almost identical among all of the three grids, the detailed temperature distributions, e.g., the ignition regions are found to be a little different, even between the results of 12.5 μm and 17 μm. Thus, although it is a little hard to conclude that a perfect grid-converged solution is obtained with the grid resolutions of 12.5 μm or 17 μm for the present condition, the present study adopts the 12.5 μm grid size, based on the results shown in Fig. 4 (a fact that the profile with 17 μm is almost identical to that with 12.5 μm) and several earlier studies [6-9].
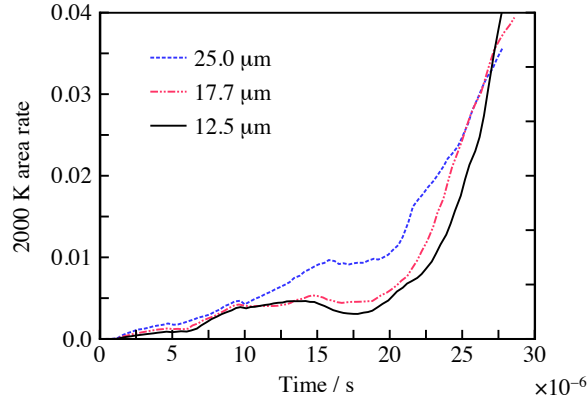
5

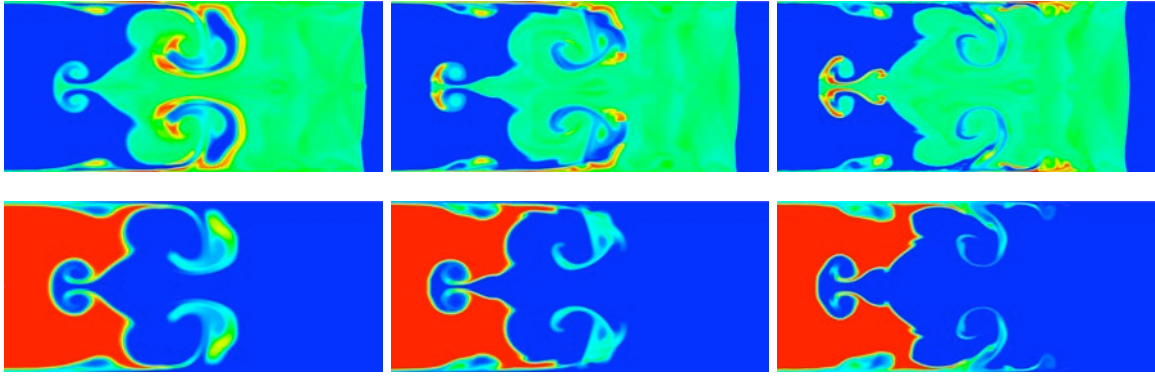Figure 4. Grid convergence study with time history of an area above 2000 K

Figure 5. Comparison of temperature (upper) and H$_2$ mass fraction (lower) distributions at t = 20.5 μs with three different grid sizes (left: Δs = 25 μm, centre: 17.7 μm, right: 12.5 μm); x = [7.187:8.305]; temperature range from 300 to 3000 K; H$_2$ mass fraction range from 0.0 to 1.0

3.4 2-D simulations: a straight diaphragm shape with no curvature

Figure 6 shows a temperature distribution at t = 31 μs and a schematic of the flow filed in the case of δ = 0.0: an initial pressure boundary with no curvature. While the one-dimensional simulation shows no ignition, the two-dimensional simulation gives an ignition occurred near the wall (although one might be difficult to recognize it in this figure due to very small region). Due to the assumption of adiabatic wall condition, the temperature at the wall takes a larger value (above 1500 K) than that behind the shock wave (about 1320 K). Therefore, the ignition rapidly occurs near the wall along with the sufficient mixing between the shock-heated air and hydrogen. On the other hand, within a length of the present duct, no ignition occurs at the contact region, which is a consistent result with the one-dimensional simulation shown in Fig. 2. Figure 7 shows the maximum temperature history obtained by the simulations with and without chemical reaction (where the reaction rate is assumed to be zero), where the high temperature value near the wall due to the adiabatic wall condition is conformed.
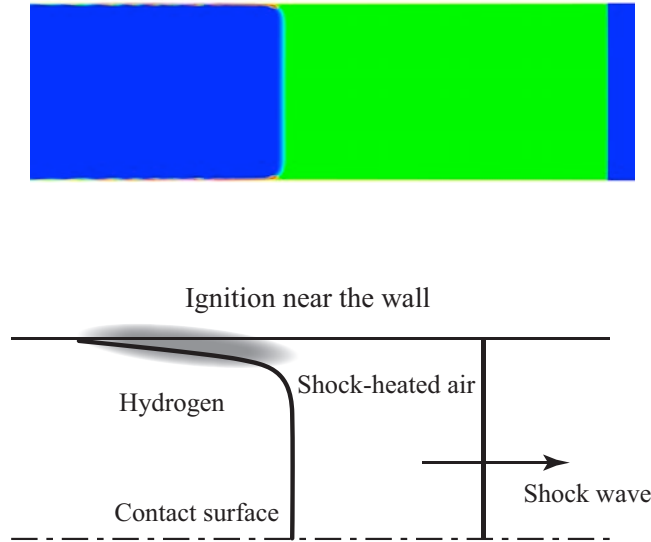
6

Figure 6. Temperature distribution at t = 32.1 μs (upper); temperature range from 300 to 3000 K x = [8.285:10.0]; and a schematic of the flow filed (lower)
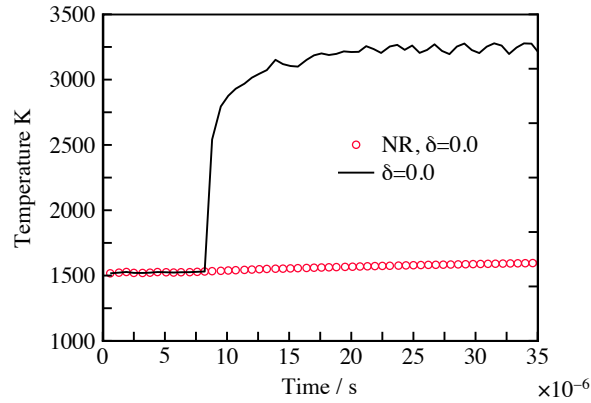

Figure 7. Maximum temperature history with δ = 0.0, where NR denotes a computational result without chemical reaction
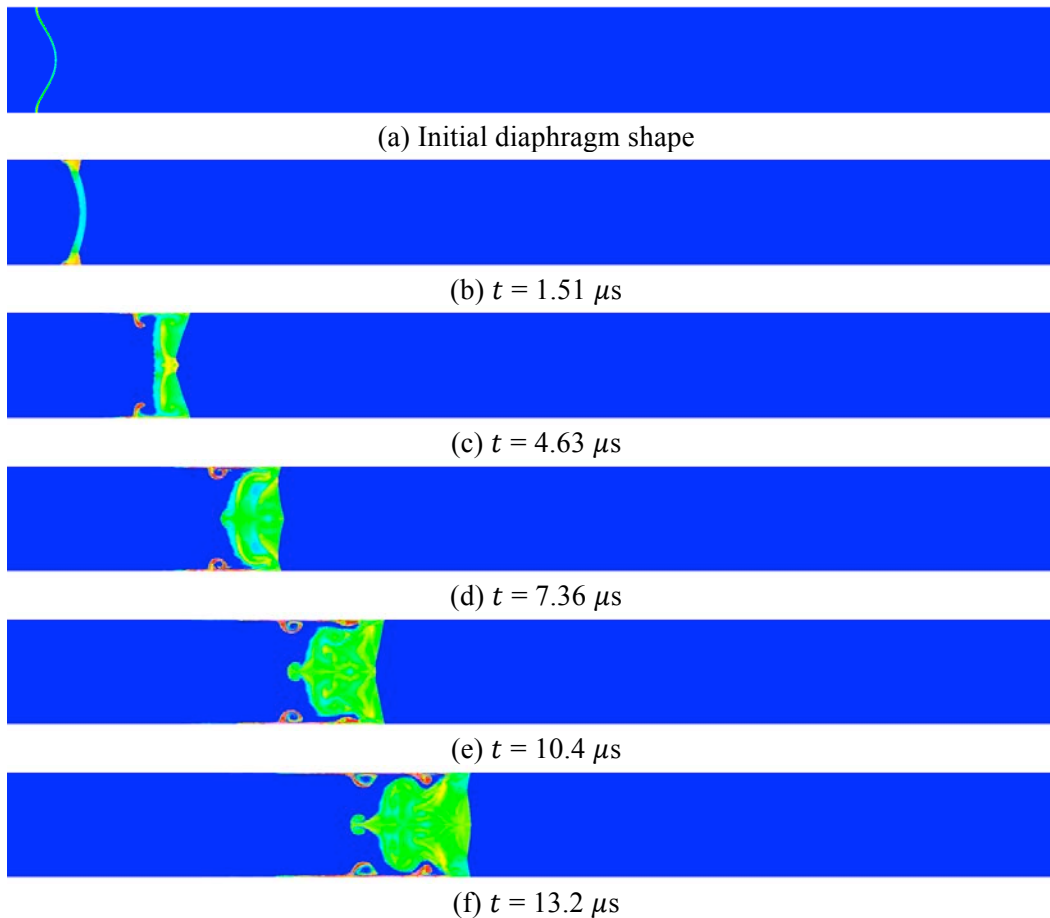
3.5 Effect of initial diaphragm shape

The sequential temperature distributions between 0.0 and 28.4 μs are shown in Fig. 8 for an initial diaphragm shape of δ = 0.1: a convex shape with the largest curvature in the present simulations. The results show that the first ignition occurs near the wall at around t = 1.5 μs as shown in Fig. 8 (b) due to the interaction of the leading shock wave with the wall. Just after the rupture, the leading shock wave is reflected at the wall, forming the Mach stem structure. Consequently, the hot temperature region more than 2000 K is produced near the wall, which is a quite higher value than that behind the leading shock wave of about 1300 K (A schematic of the flow fields described is given in Fig. 9). Figure 9 shows the maximum temperature histories obtained with and without chemical reaction. It is found that, even if no chemical reaction is considered, the maximum temperature goes up to about 2100 K at the early stage, which also indicates the occurrence of strong compression due to the Mach stem structure. Thus, hydrogen and air are instantly ignited due to such high temperature spot.

The secondary ignition takes place in the boundary layer during 7.3 ~ 10.4 μs as shown in Figs. 8 (d) and 8 (e). A schematic of the secondary ignition is given in Fig. 10. The deformed shock wave and contact surface gradually become flat as the flow moves downstream. The vorticity is thereby generated (clockwise direction in the upper half region, and vice versa), which produces a flow stream

7

of hydrogen into the shock-heated air region. The incoming hydrogen meets the shock-heated air remained in the boundary layer and the ignition is induced. This secondary ignition can be recognized with the time history of the 2000 K area rate shown in the upper figure of Fig. 10. It is found that the 2000 K area gradually increases around $t = 8.0\ \mu s$ and keeps the value until about $t = 20.0\ \mu s$, followed by third ignition described next.

The third ignition is seemingly a catastrophic event, a schematic of which is given in Fig. 10. The incoming hydrogen continuously penetrates deeply into the shock-heated air as shown in Figs. 8 (g) ~ 8 (i), forming a large amount of combustible contact regions. The ignition then takes place catastrophically with certain mixing and ignition delay time. The time history of the 2000 K area rate in Fig. 10 also shows the rapid increase of the high-temperature area, starting from $t = 20.0\ \mu s$. Finally, as shown in Figs. 8 (j) and 8 (k), the high-temperature burnt gas occupies the cross section of the duct.

Here, it may be worth noting some relations between high-temperature burnt-gas regions and chemical reactions in a downstream region. The reaction rate of H_2O ($\dot{\omega}_{H_2O}$) distributions is used to identify the locations where chemical reactions actively take place. Figure 11 shows a comparison between the temperature and the reaction rate of H_2O distributions at two different times. While the high-temperature burnt-gas is almost produced consistently at the high reaction rate region at an earlier time of $t = 29.8\ \mu s$, at a later time of $t = 35.1\ \mu s$, the high reaction rate region is barely matched with the high-temperature burnt-gas region. This indicates that, in the downstream region, a large amount of high-temperature burnt-gas is just flowing through without chemical reaction, i.e., occurrence of chemical reaction may decrease due to lack of mixing between unburnt hydrogen and air, potentially leading to a quenching in a downstream region.
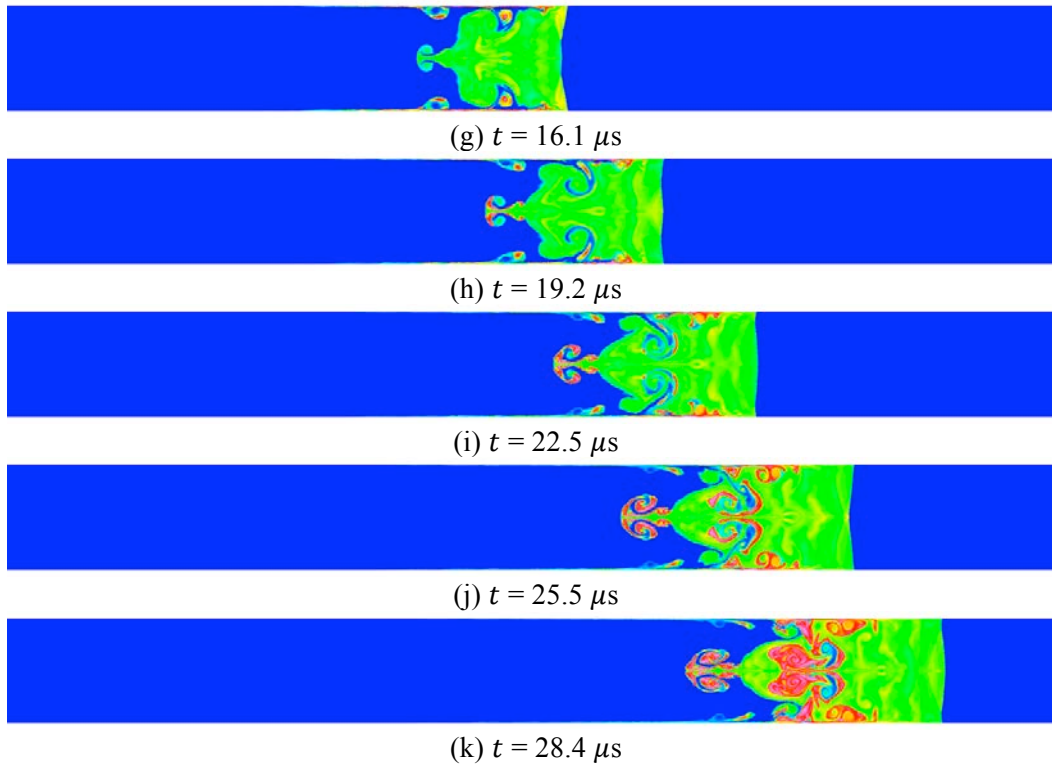

(a) Initial diaphragm shape

(b) $t = 1.51\ \mu s$

(c) $t = 4.63\ \mu s$

(d) $t = 7.36\ \mu s$

(e) $t = 10.4\ \mu s$

(f) $t = 13.2\ \mu s$

(g) t = 16.1 μs

(h) t = 19.2 μs

(i) t = 22.5 μs

(j) t = 25.5 μs

(k) t = 28.4 μs

Figure 8. Sequential temperature distributions with δ = 0.1; x = [4.87:10.0]; temperature from 300 to 3000 K
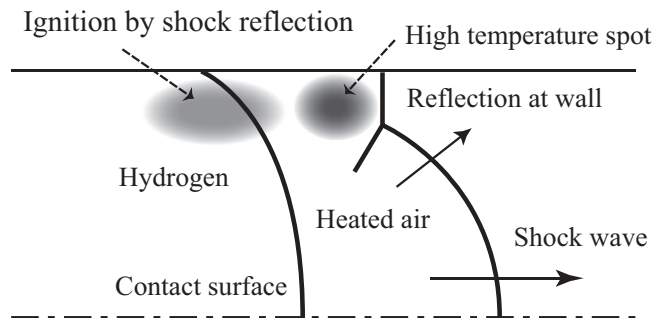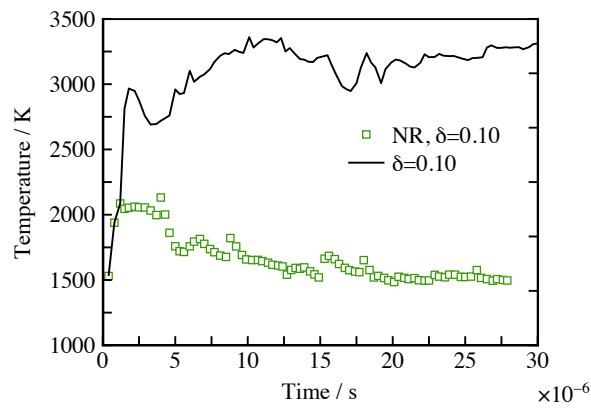

Figure 9. Maximum temperature history with δ = 0.1, where NR denotes a computational result without chemical reaction (upper) and a schematic of the first ignition (lower)
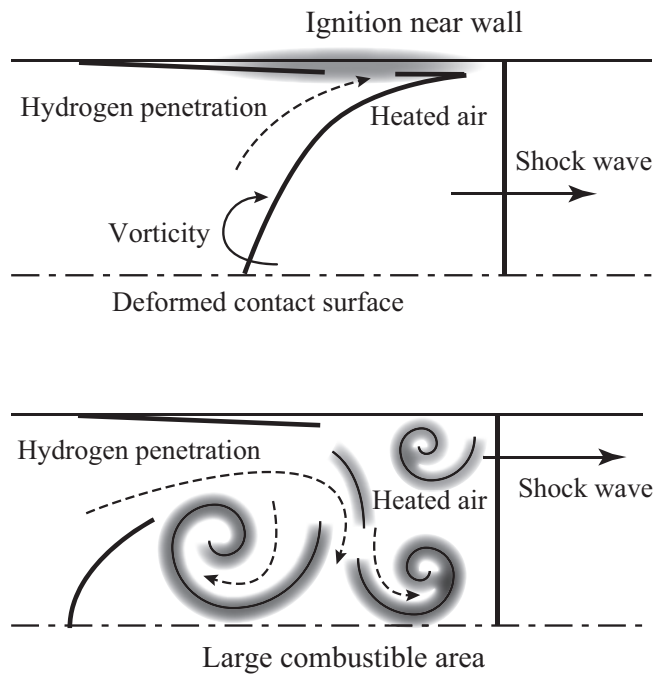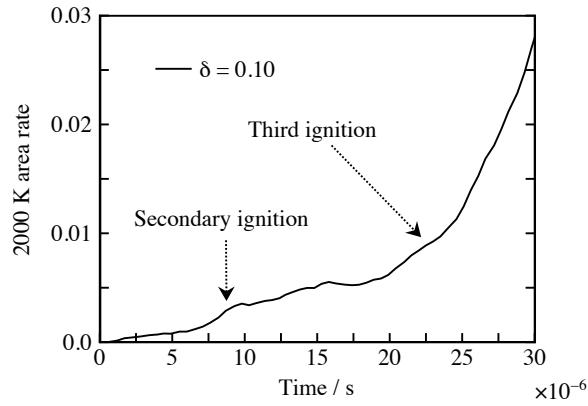
9

Figure 10. Time history of an area above 2000 K with δ = 0.1 (upper), a schematic of the secondary ignition (middle), and that of the third ignition (lower)
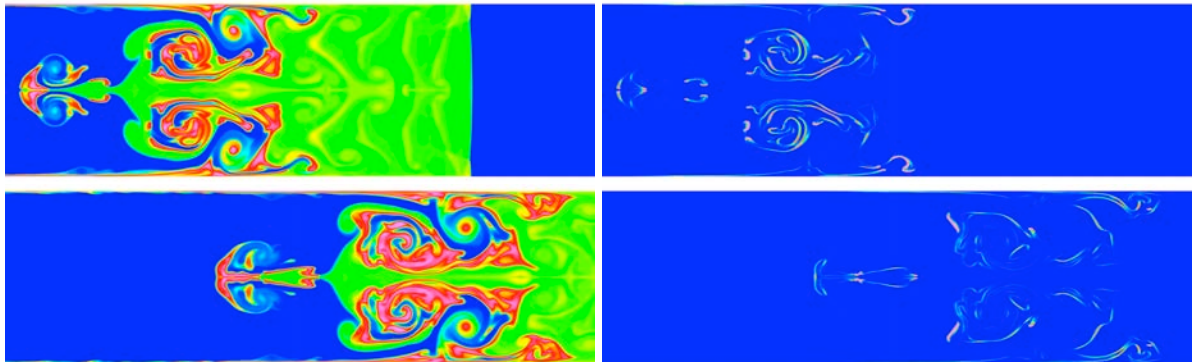

Figure 11. Temperature (left) and reaction rate of H_2O (right) distributions at t = 29.8 μs (upper) and t = 35.1 μs (lower); x = [8.285:10.0]; temperature from 300 to 3000 K; reaction rate from 0.0 to 30.0

In the case of $\delta = 0.05$, the hydrogen cannot penetrate deeply into the shock-heated air due to weaker vorticity as shown in Fig. 12, where the timing of snapshot ($t = 28.4 \mu$s) is the same as that in Fig. 11. It is found that the initial diaphragm shape strongly influences the following vortical structure and the temperature distribution in the downstream region. The 2000 K area rate in Fig. 12 also shows the large difference appears in the production of combustible area due to the initial diaphragm shape.
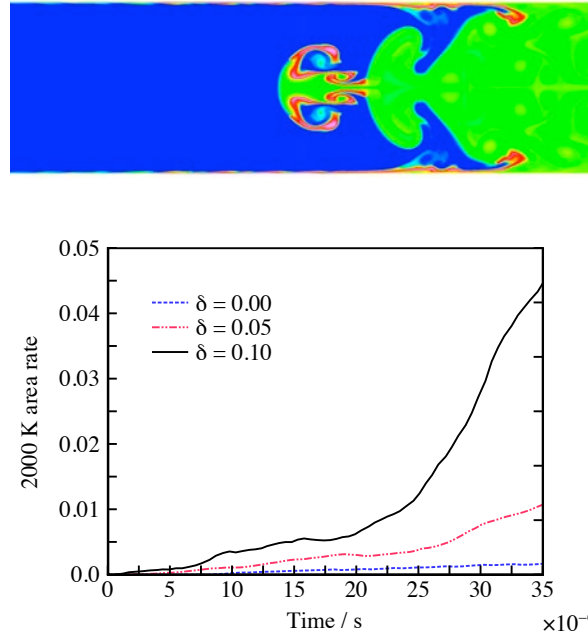

Figure 12. Temperature distributions at $t = 35.1 \mu$s with $\delta = 0.05$ (upper) where the results with $\delta = 0.0$ and 0.1 are plotted for comparison; $x = [8.285:10.0]$; temperature from 300 to 3000 K and time history of an area above 2000 K (lower)

4.0 CONCLUSIONS

Spontaneous ignition of high-pressure hydrogen released into air has been simulated in a manner of direct numerical simulation in order to explore its underlying ignition mechanisms. The present study adopts 2-dimensional rectangular duct geometry and focuses on the effect of initial diaphragm shapes on the mechanism of spontaneous ignition. The preliminary 0- and 1-dimensional simulations provide a fact that no ignition occurs at the contact surface in a length of the present duct. In contrast, for the two-dimensional simulation, the ignition occurs with any initial diaphragm shape due to the appearances of wall condition and 2-dimensional mixing structures. In the case of $\delta = 0.0$, the ignition occurs only near the wall due to the use of adiabatic wall condition. In the case of $\delta = 0.1$, the three ignition events are identified; the first ignition is induced by the shock wave reflection at the wall, the secondary ignition occurs due to the hydrogen penetration into the shock-heated air near the wall, and the third ignition takes place catastrophically in the entire cross section of the duct due to the deep penetration of hydrogen into the shock-heated air. The present study thus demonstrates the significant importance of initial diaphragm shape on the spontaneous ignitions, clarifying the detailed mechanisms.

REFERENCES

1. Wolanski, P. and Wojcicki, S., *Proc. Combust. Inst.*, **14**, 1973, pp. 1217-1223.
2. Dryer, F.L., Chaos, M., Zhao, V., Stein J.N., Alpert, J.Y. and Homer, C.J., *Combust. Sci. Tech.*, **179**, 2007, pp. 663-694.
3. Golub, V.V., Baklanov, D.I., Golovastov, S.V., Ivanov, M.F. Laskin, I.N. and Saveliev, A.S., *J. Loss Prevent. Proc.*, **21**, 2008, pp. 185-198.

4. Mogi. T., Kim, D., Shiina, H. and Horiguchi, S., *J. Loss Prevent. Proc.*, **21**, 2008, pp. 199-204.

5. Kim. Y.R., Lee. H.J., Kim. S. and Jeung. I.S., *Proc. Combust. Inst.*, **34**, 2013, pp. 2057-2064.

6. Wen, J.X., Xu, B.P. and Tam, V.H.Y., *Combust. Flame*, **156**, 2009, pp. 2173-2189.

7. Xu, B.P. and Wen, J.X., *Int. J. Hydrogen Energy*, **37**, 2012, pp. 17571-17579.

8. Lee, B.J. and Jeung. I.S., *Int. J. Hydrogen Energy*, **34**, 2009, pp. 8763-8769.

9. Yamada. E., Kitabayashi. N., Hayashi. A.K. and Tsuboi. N., *Int. J. Hydrogen Energy*, **36**, 2011, pp. 2560-2566.

10. Bragin. M.V. and Molkov. V.V., *Int. J. Hydrogen Energy*, **36**, 2011, pp. 2589-2596.

11. Toro. E.F., Spruce. M. and Speares. W., *Shock Waves*, **4**, 1994, pp. 25-34.

12. Kim. S.D., Lee. B.J., Lee. H.J. and Jeung. I.S., *J. Comput. Physics*., **228**, 2009, pp. 7634-7642.

13. van Leer, V, International Conference on Numerical Methods in Fluid Dynamics, 1982, pp. 507-512.

14. Gottlieb. S. and Shu. C.W., *Math. Comput.,* **67**, 1998, pp. 73-85.

15. Hirschfelder, J.O., Curtiss. C.F. and Bird. R.B., Molecular Theory of Gases and Liquids, 1954, John Wiley and Sons, Inc., New York.

16. Warnatz, J., Numerical Methods in Flame Propagation, Eds N. Peters and J. Warnatz, Friedr, 1982, Vieweg and Sohn, Wiesbaden.

17. Bird, R.B., Stewart. W.E. and Lightfoot. E.N., Transport Phenomena, 1960, John Wiley and Sons, Inc., New York.

18. Mathur. S., Tondon. P.K. and Saxena. S.C., *Mol. Phys*., **12**, 1967, pp. 569.

19. Gou. X., Sun. W., Chen. Z. and Ju. Y., *Combust. Flame*, **157**, 2010, pp. 1111-1121.

20. Brown. P.N., Byme. G.D. and Hindmarsh. A.C., *SIAM J. Sci. Stat.,* **10**, 1989, pp. 1038-1051.

21. Shimizu. K., Hibi. A., Koshi. M., Morii. Y. and Tsuboi. N., *J. Propulsion Power* **27**, 2011, pp. 383-395.